Advances in Applied Ceramics, Volume 112, Issue 1 (January 2013), pp. 53-58

Impact of crystallisation processes on depth profile formation in sol-gel $PbZr_{0.52}Ti_{0.48}O_3$ thin films

I. Aulika[1], S. Mergen[2], A. Bencan[3], Q. Zhang[4], A. Dejneka[5], M. Kosec[3]

[1] *Center for Space Human Robotics @PoliTO, Italian Institute of Technology, Turin, Italy, email: ilze.aulika@iit.it*
[2] *HEARing CRC, University of Melbourn, Australia*
[3] *"Jožef Stefan" Institute, Ljubljana, Slovenia*
[4] *Cranfield University, School of Applied Sciences, Cranfield, UK*
[5] *Institute of Physics, Academy of Science, Prague, Czech Republic*

Abstract: This study revealed the influence of crystallization processes on the homogeneity of the sol-gel $PbZr_{0.52}Ti_{0.48}O_3$ thin films, allowing identification and further optimization of thin film performance. Crystallization processes determine the optical gradient appearance, irrespective of the chemical solvents used in this work. XRD analysis shown that a refractive index gradient was apparent in the samples which had dominant (001)/(100) orientation and significant change of lattice parameters with thickness.
Keywords: Compositional and optical gradient, depth profile, PZT, thin films, sol-gel, crystallisation process, XRD, spectroscopic ellipsometry.

1. Introduction

The growing interest in compositionally graded ferroelectric (FE) films for improved piezoelectric properties [1], the dielectric analogue based on polarisation-graded FE for the transistor (i.e., trans-capacitive (transpactitive) devises and structures) [2], and adaptive FE memories for space applications [3] make it imperative to study the depth profile of thin films throughout a single layer and an entire coating. $Pb(Zr_xTi_{1-x})O_3$ (PZT) films have formed an integral part of the microelectromechanical systems (MEMS) in various applications, which requires a different thickness of the functional film and homogeneity control, leading to the challenge of manufacturing the film of the required thickness and quality. Among many methods for the PZT thin film fabrication, chemical solution deposition (CSD) methods offer low-capital costs and relatively easy control of chemical composition and homogeneity [4]. Nevertheless, information on the homogeneity of the films and the physical properties resulting from CSD processing methods represents crucial knowledge, especially since gradients in optical properties and chemical composition have been reported previously for CSD-fabricated PZT films [1, 5-8], but its origin has not been elucidated. It is not clear if the chemical route or the crystallization process is responsible for the chemical concentration gradients.

Variation of chemical composition throughout the film thickness results in variation of physical properties of the films and lowers [4, 5] or improves [1] the performance of electromechanical systems. Due to the proportionality of the refractive index to the square of the spontaneous polarization, the inhomogeneity of the film can be detected as a variation of refractive index within the depth of the film (optical depth profile) [10, 11]. It is known that with the increase of Zr/Ti ratio refractive index *n* decreases [4, 9]. The presence of excess Pb also leads to the change of *n*. Fig. 1 illustrates, in a simplified way, the relation of compositional and optical depth. On the other hand, any change in FE material structure will affect the polarization and thus optical properties of the material, irrespective of whether it is a result of the stoichiometry, compositional gradient, internal stresses, etc.

A challenging aspect of studying compositional homogeneity in PZT thin filmslies in the identification of compositional gradients within a film. The compositional gradients can

be detected using Z contrast transmission electron microscope (TEM) with energy dispersive x-ray spectroscopy (EDX), but it requires specific sample preparation. Investigation using other methods such as Rutherford back-scattering (RBS) results in sample modification or even destruction after analysis. Furthermore, such methods suffer from being ''local'', intrusive, and destructive. On the other hand, contactless optical methods such as spectroscopic ellipsometry (SE) allow one estimating the film homogeneity (for example, optical depth profile [10-17]) without specific sample preparation requirements.

In this study, we present results on optical depth profile of sol-gel $PbZr_{0.52}Ti_{0.48}O_3$ (PZT 52/48) thin films made with two widely used sol-gel routes and using two different approaches of crystallisation, which in turn would allow conclusions about chemical composition gradients. The overview of how the film orientation changes when more layers are added has been obtained, giving more understanding on crystallisation processes in sol-gel PZT.

2. Experimental

Sol-gel $PbZr_{0.52}T_{0.48}O_3$ (PZT 52/48) thin films were made by using two different solvent systems: a mixture of acetic acid and methanol (AcOH/MeOH) or 2-Methoxyethanol (2-MEO). Details of route preparation can be found in Ref. [18, 19]. Two different thermal profiles were applied to crystallize the films: (i) all layers crystallized together at the same time (LCT), and (ii) each layer crystallized individually (LCI). The first profile employed the deposition of one layer followed by drying at 300°C for 1 min. When the final layer was deposited, the sample was placed on a hotplate at 550°C for 35 min to crystallize. The second thermal profile involved individual crystallization of each layer by holding the sample at 300°C for 1 min followed by 550°C for 5 min before the next layer was coated. For each possible combination of thermal profile and sol, a series of 4 sample groups was made, with each film having between 1 and 5 layers. The list of samples is summarized in Table 1.

The crystallographic structure and out-of-plane orientation of each film was determined by the standard θ-2θ X-ray diffraction (XRD) method using a Siemens D5005 diffractometer with CuKα radiation and a Goebel mirror. Variable angle spectroscopic ellipsometry (VASE) was performed using a J. A. Woollam Co VASE spectroscopic ellipsometer. Optical depth profile was modelled using exponential and polynomial variation of refractive index at 700 nm [19]. Thin film structures were characterized by a TEM (JEM 2010F FEG-AEM), operated at 200 kV accelerating voltage. The chemical composition was investigated using a LINK ISIS 300 EDX spectrometer and a Si–Li detector.

3. Results and discussion

3.1. Optical depth profile

Among all analyzed samples, the change of the refractive index n with the film thickness d was found only in the films made by crystallizing each individual layer (LCI). No optical gradient was found in the films in which all layers were crystallised together (LCT). The films made by using AcOH/MeOH sol (Fig. 2a) have more complex optical gradient comparing with the films made by using 2-MEO sol (Fig. 2b). For all films made by using AcOH/MeOH sol, the first layer has the gradient at the interface to the next layer. $n(d)$ decreases throughout the second layer for two layer films. The third layer shows a slight increase in $n(d)$, but after adding the fourth and fifth layer, the second and third layer converge. Such differences in $n(d)$ from one film to another is most likely due to recurrent annealing of already crystallized layers, causing the diffusion of Pb, Ti and Zr ions in the film. For all films made by using 2-MEO sol, n increases towards the film surface. The reasons for the $n(d)$ change may be: (i) residual stress in the film, (ii) concentration gradients of Ti, Zr or Pb with the layer.

It is demonstrated that *n* increases with decreasing Zr/Ti ratio [9]. If we extrapolate this relation (Fig. 1) to the optical depth profile, e.g., given in Fig. 2b, it can be speculated that Zr/Ti ratio decreases directionally from the substrate to the surface. However, it is known that sol-gel thin films may have higher concentrations of Pb at the surface [1, 6, 20]. The experiments of Watts *et al* [20] and Impey *et al* [6] suggest that the diffusion of lead to the surface in PZT films results from oxidation of the Pb or from kinetic demixing, both of which would be favoured by incomplete oxidation of the film during deposition. Pb^{2+} diffusion may also lead to self-polarization, which causes the polarization inhomogeneity [21].

3.2. X-ray diffraction

The AcOH/MeOH and 2-MEO LCI samples (Fig. 3ac) show a dominant (001)/(100) orientation. (111) peaks were observed in AcOH/MeOH samples having three or more layers (Fig. 3a), however, the intensity of these peaks is rather small compared to (100) peaks. For all these samples a pronounced optical depth profile was found (Fig. 2).

The XRD results for the AcOH/MeOH and 2-MEO LCT samples show more mixed orientation (Fig. 3bd). AcOH/MeOH samples have dominant (111) peak and additional (110) and (001)/(100) peaks (Fig. 3b). The films made with 2-MEO sol also have the (111) peak, but it appears only in the samples with three or more layers (Fig. 3d): the first two samples (with 1 and 2 layers) were strongly (001)/(100) oriented. Interestingly, no optical gradient is found for LCT samples. For these films the nucleation and crystallization are strongly dictated by the substrate, due to the lattice match between PZT(111) and Pt(111).

It must be noted that since LCT films were crystallized only when the last layer was deposited, the samples do not represent a sequential change in orientation with increasing number of layers, but rather, each sample stands on its own, showing the influence of the total film thickness on film crystallization. The situation is different for LCI samples: based on these XRD results, we obtain a picture of how the orientation of the film changes when more layers are added, assuming a reproducible orientation. Thus, when processing the films using the LCI method, only the first layer crystallizes directly on the Pt substrate and all subsequently deposited layers crystallize on top of the former layer. Since the thermal profile used assures (100) orientation of the film, we would expect the first layer to be (100) oriented, as well as all subsequently deposited layers, since the last layer also is crystallize on (100) PZT. Nevertheless, both groups of PZT 52/48 films processed with the LCI method exhibit some (111) orientation for films having more than three layers.

The growth of PZT 52/48 films with (100) orientation when pyrolysed at 300°C was reported earlier by Marshall *et al* [22] using an AcOH/MeOH sol and the LCI method. The (100) nucleation on the Pt(111) substrate is likely to take place in the presence of high lead excess and in the pyrolysis temperature range between 300°C and 350°C. The competing nucleation of PZT(111) is hindered due to high PbO content and is only enabled at higher temperatures where PbO volatility is increased. Thus, once the PbO is removed from the film, the formation of the intermetallic phase Pb_3Pt that facilitates the (111) nucleation is enabled, as observed on PZT 30/70 films [23].

The appearance of (111) orientation was also observed in the work of Brennecka et al [8]: after crystallization the excess of PbO was found near the surface. Indeed, some pyrochlore was found for all LCI films made with AcOH/MeOH sol (Fig. 3a, Tab.1). It is thus possible that after the deposition of the next layer, the residual pyrochlore induced nucleation and growth in the (111) direction, consuming the uncrystallized matrix and accounting for the appearance of the (111) orientation at later stages within the first layer. Considering the work of Brennecka *et al*, the uncrystallized pyrochlore phase was most likely the lead deficient fluorite phase, which was also accompanied by a compositional gradient of Pb/Zr through the layer thickness in their work.

The presence of compositional gradient can be seen as the significant change of refractive index within the film (Fig. 2). It was especially pronounced at the interfaces between the layers for the AcOH/MeOH sol samples from 2 up to 5 layers (Fig. 2a). For these samples the (111) peak is also present in XRD spectra (Fig. 3a). Thick interface layers between Pt and PZT (~ 6÷10 nm), and significant surface roughness (~ 7÷10 nm) were detected using SE for all LCI samples what can be related to the existence of the intermetallic phase Pb_3Pt and the lead deficient fluorite phase.

The reduction of initially high tensile stress with increasing thickness correlates to the observed peak shift toward smaller 2Θ in the XRD (see magnified (002)/(200) peaks in Fig. 3ac, and (002) and (022) peak position in Fig. 4). The peak shift indicates the increase of lattice spacing in the out-of-plane direction, which is likely to be accompanied by the decrease of lattice spacing in-plane. However, our data is rather limited and does not allow conclusions as to whether initially high tensile stress (in plane) decreased, or whether it further increased upon the deposition of more layers. It was observed earlier that the presence of pyrochlore is accompanied by large tensile stress. The presence of stress and the variation of stress with film thickness are reflected in the variation of lattice parameters for each film. In the first layer of AcOH/MeOH LCI samples, the lattice spacing was 0.4052Å and 0.4037Å for (002) and (200), respectively. This parameter was found to increase with increasing number of layers up to 0.408Å and 0.4047Å, respectively. This is equivalent to an elongation of 0.7%. Initial high tensile stress in thin films, which decreases upon further layer deposition, was observed previously for PZT 52/48 films [24].

Besides that all films made with LCI processing showed pronounced (001)/(100) orientation, there were differences between AcOH/MeOH and 2-MEO samples based on the shift of (002)/(200) peaks. For 2-MEO films, the (002) peak shifts to smaller 2Θ angles, whereas the (200) peak shifts to higher 2Θ angles; in other words, the peaks drift apart from each other (see Fig. 4). This indicates that the tetragonal split (002)/(200) increases with increasing film thickness and is hence more pronounced. It suggests that with increasing numbers of layers, and thus heat treatments, stress relaxation, defect healing and improvement of crystallographic structure can occur in each underlying and already crystallized layer. The c/a ratio for these films is 1.008, which is the highest between all films. The 2-MEO films were also all completely crystallized. For these films no pyrochlore phase was found, which would induce nucleation and growth in the (111) direction. The change of *n* within the film can be related to the variation of Zr/Ti and/or tensile stresses.

3.3 TEM analysis

The cross-section of 3 layer film made by using AcOH/MeOH sol and LCI, for which a strong optical gradient was found (Fig. 2a), is presented in Fig. 5a. It shows fine grains of pyrochlore phase between perovskite crystallites throughout the film thickness, and a pyrochlore layer about 50 nm thick at the surface of the film. These results are in accordance with the XRD analysis (Fig. 3a). Close to the surface where the pyrochlore layer was observed, a strong reduction in Pb concentration and an increase in Zr concentration were detected by EDX. The Ti concentration was not much affected by the phase separation. The reduction of Pb concentration is present in the optical depth profile of the films as decrease of refractive index in the second layer of the film (Fig. 2a). Due to the similarities in the sol composition and processing between our work and the work of Brennecka *et al*, we can conclude that this sample shows the same two-phase structure reported by Brennecka *et al* within each layer, whereby the lead-deficient in upper layers causes a compositional gradient.

The cross section of 3 layer film made using AcOH/MeOH sol and LCT is shown in Fig. 5b. Columnar grains and ~10 nm thin pyrochlore layer on the surface was found. No Py was detected by XRD analysis due to its low amount (see Fig. 3b), but it is present in the

selected area electron diffraction (SAED) image (Fig. 5b). No changes in Pb, Zr and Ti concentration were detected by EDX and no optical gradient was found by SE.

4. Summery

The depth profile of the refractive index is established for PZT 52/48 thin films made with LCI irrespective of the chemical solvent type. The analysis of the XRD results of PZT 52/48 films made with LCI has shown that these films have a preferred orientation of (001)/(100) in contrast to the films made with LCT, which have shown a predominant (111) orientation and no gradient in optical properties. A more refined XRD analysis presented that an optical gradient was apparent in the samples in which lattice parameters strongly change with thickness. For these films, EDX analysis showed significant variation in Pb and Zr.

Separate crystallization of the layers determines the gradient appearance, irrespective of the chemical solvents used in this work. Variation in Zr/Ti ratio in PZT films originates early in the crystallization process. These variations are caused by a mismatch in the thermal decomposition of the individual Zr/Ti components in the PZT precursor. Once created, the compositional gradients cannot be eradicated by prolonged heat treatments. Selection of precursors (chemical solvents) and processing parameters (drying temperatures and time, crystallization temperature and time, etc.) for the deposition of sol-gel films is influential in controlling the homogeneity of the films.

5. Acknowledgements

This work was supported by tge grants KAN301370701 of the ASCR, 1M06002 of the MSMT CR, 2 202/09/J017 of GACR and AV0Z10100522. We would like to express our gratitude to Sebastjan Glinsek for TEM sample preparation.

6. References

[1] N. Ledermann, P. Muralt, J. Baborowski, S. Gentil, K. Mukati, M. Cantoni, A. Seifert and N. Setter: *Sens. Actuators A,* 2003, 105, 162**.**

[2] Joseph. V. Mantese, S. Pamir Alpay: *Graded ferroelectrics, transpacitors and transponents*, Springer Sciece+Businedd Media, NY, 2005; Z.-G. Ban, S. P. Alpay and J. V. Mantese: *Phys. Rev. B,* 2003, 67, 184104.

[3] D. A Kamp, A. D. DeVilbiss, S. C. Philpy, G. F. Derbenwick, *IEEE, Non-Volatile Memory Technology Symposium*, 2004, 10.1109/NVMT.2004.1380832.

[4] N. Izyumskaya, Y.-I. Alivov, S.-J. Cho, and H. Morkoc, H. Lee, Y.-S. Kang: *Crit. Rev. Solid State Mater. Sci*., 2007, 32, 111.

[5] A.Etin, G. E. Shter, S. Baltianski, and G. S. Grader: *J. Am. Ceram. Soc.,* 2006, 89, 2387**.**

[6] S. A. Impey, Z. Huang, A. Patel, R. Beanland, and N. M. Shorrocks, R. Watton, R. W. Whatmore: *J. Appl. Phys*., 1998, 83, 2202**.**

[7] F. Calamea and P. Muralt: *Appl. Phys. Lett*., 2007, 90, 062907.

[8] G.L. Brennecka, C. M. Parish, B. A. Tuttle, L. N. Brewer, M.A. Rodriguez: *Adv. Mater*., 2008, 20, 1407.

[9] C. M. Foster, G.-R. Bai, R. Csencsits, J. Vetrone, R. Jammy, L. A. Wills, E. Carr, and J. Amano: *J. Appl. Phys*., 1997, 81, 2349.

[10] A. Deineka; M. D. Glinchuk; L. Jastrabik; G. Suchaneck; G. Gerlach: *Ferroelectrics,* 2001, 264, 151; G. Suchaneck, W. -M. Lin, R. Koehler, T. Sandner, G. Gerlach, R. Krawietz, W. Pompe, A. Deineka, L. Jastrabik: *Vacuum,* 2002, 66, 473**.**

[11] I. Aulika, A. Dejneka, V. Zauls, K. Kundzins: *J. Electrochem. Soc*., 2008, 155, G209.

[12] H. G. Tompkins, E. A. Irene: *Handbook of ellipsometry*, NY, 2005.

[13] J. Rivory: *Thin Solid Films,* 1998, 313-314, 333.

[14] H. Nishizawa, Y. Tateyama, T. Saitoh: *Thin Solid Films* 2004, 455-456, 491.

[15] M. Losurdo: *Thin Solid Films* 2004, 455-456, 301**.**

[16] D. E. Morton, B. Johs and J. Hale: *Soc. of Vac. Coat. 505/856-7188, 45th Ann. Techn. Conf. Proc*. 2002, ISSN 0737-5921, 1**.**
[17] M. Fried, P. Petrik, T. Lohner, N. Q. Khánh, O. Polgár and J. Gyulai: *Thin Solid Films,* 2004, 455-456, 404**.**
[18] Q. Zhang, Z. Huang and R.W. Whatmore: *J. Sol-Gel Sci. Technol*., 2002, 23, 135.
[19] I. Aulika, S. Corkovic, A. Bencan, S. D'Astorg, A. Dejneka, Q. Zhang, M. Kosec and V. Zauls: *Journal of Electrochemical Society,* 2009, 156, G217.
[20] B. E. Watts, F. Leccabue, G. Bocelli, G. Padeletti, S. Kaciulis, L. Pandolfi: *J. Eur. Ceram. Soc.,* 2005, 25, 2495.
[21] M. D. Glinchuk, E. A. Eliseev, and V. A. Stephanovich: *Physica B,* 2002, 322, 356.
[22] J. M. Marshall, S. Corkovic, Q. Zhang, R. W. Whatmore, C. Chima-Okereke, W. L. Roberts, A. J. Bushby, M. J. Reece: *Integrated Ferroelectrics,* 2006, 80, 77**.**
[23] Z. Huang, Q. Zhang, R. W. Whatmore*: J. App. Phys*. 1999, 86, 1662**.**
[24] S. Corkovic, R. W. Whatmore, Q. Zhang: *J. Appl. Phys***.,** 2008, 103, 084101**.**

Tab. 1. Information on PZT 52/48 films: sol-gel solvent, crystallization process (LCT or LCI), amount of the layers annealing temperature, and observed peaks of XRD.

Fig. 1. Illustrative relation between the compositional (Ti/Zr and Pb) and refractive index variation within the film.
Fig. 2. Depth profile at the 700 nm for the samples with different number of layers made using LCI and a) AcOH/MeOH, and b) 2-MEO sol.
Fig. 3. The XRD of a) AcOH/MeOH and LCI films, b) AcOH/MeOH and LCT films from, c) 2-MEO and LCI films, and d) 2-MEO and LCT films. The magnification of (002)/(200) peaks (a, c).
Fig. 4. The shift of (002) and (200) peak position after adding additional layers of the LCI films.
Fig. 5. TEM micrograph (bright field) of a cross-section of a) LCI and b) LCT film showing pyrochlore phase (Py) on the surface (a, c) and between the grains (a) of the PZT films. Bellow: SAED of the PZT grains of a) LCI and b) LCT samples in 0-21 zone axis. Diffused marked ring is due to Py at the surface.

Tab. 1

Nr	Solvent	Crystallisation process	Number of samples	Annealing (pyrolyses/crystallisation)	X-ray		
1	AcOH/MeOH	LCT	5 samples 1 ÷ 5 layers 100 nm/layer	300°C, 1 min 550°C, 35 min	1	**(100)**, **(200)**	
					3	(100), **(110)**, **(111)**, (200)	
					5	(100), **(110)**, **(111)**, (200)	
2							
		LCI	5 samples 1 ÷ 5 layers 110 nm/layer	300°C, 1 min 550°C, 5 min	1	**(100)**, **(200)**	
					3	**(100)**, (111), **(200)**	Py
					5	**(100)**, **(111)**, **(200)**	
3	2-MEO						
		LCT	5 samples 1 ÷ 5 layers 68 nm/layer	300°C, 1 min 550 °C, 35 min	1	**(110)**, (110), **(200)**	
					3	(110), (110), (111), (200)	
					5	(110), (110), **(111)**, (200)	Py
4							
		LCI	5 samples 1 ÷ 5 layers 65 nm/layer	300°C, 1 min 550°C, 5 min Final: 550°C for 30 min	1	**(100)**, (111), **(200)**	
					3	**(100)**, (111), **(200)**	
					5	**(100)**, (111), **(200)**	

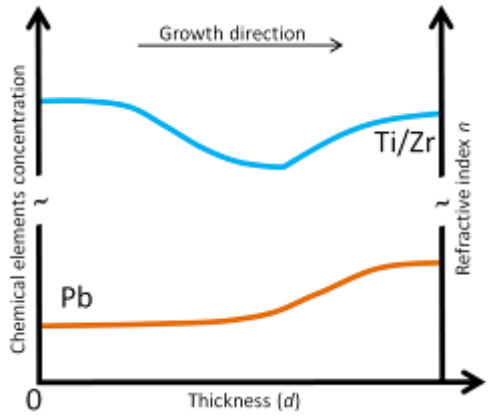

Fig. 1.

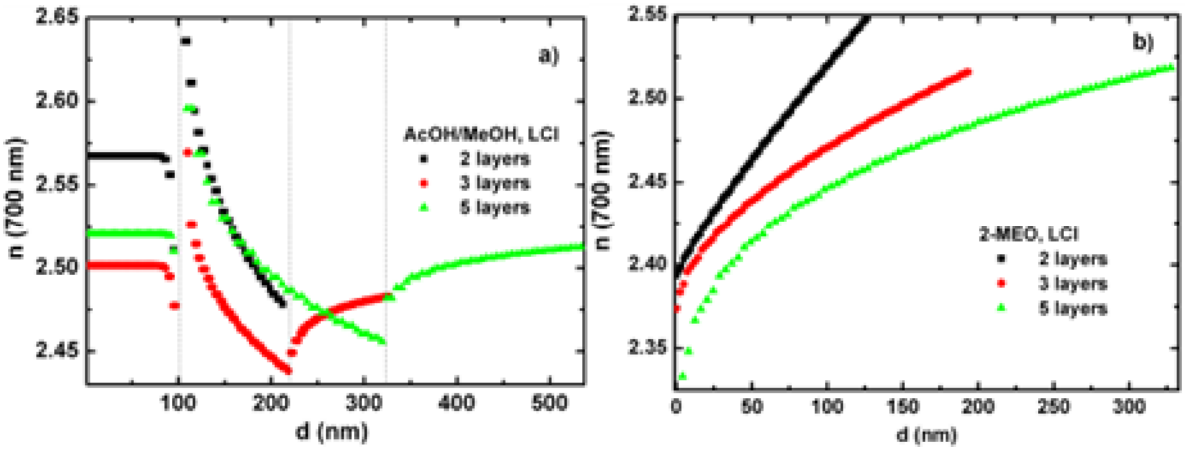

Fig. 2.

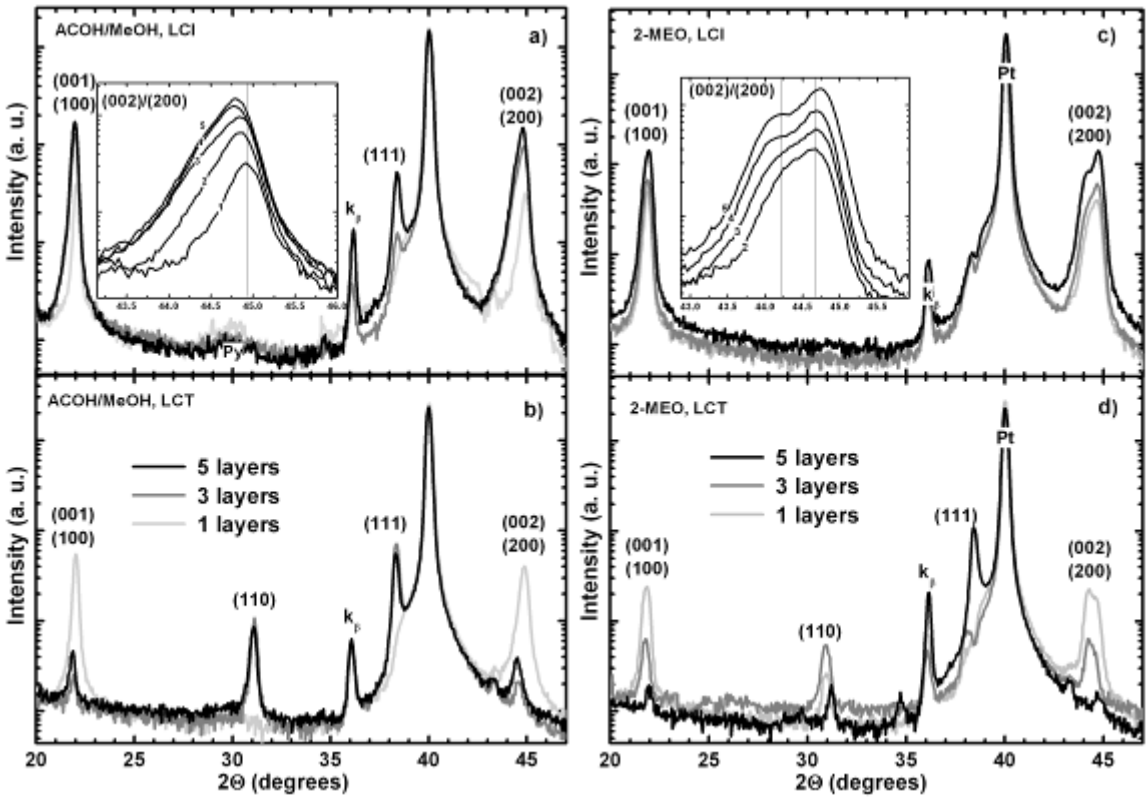
ACOH/MeOH, LCI
a)
(001)
(100)
(002)/(200)
(111)
(002)
(200)
Py
Intensity (a. u.)
2-MEO, LCI
c)
Pt
ACOH/MeOH, LCT
b)
5 layers
3 layers
1 layers
(110)
2-MEO, LCT
d)
2Θ (degrees)

Fig. 3.

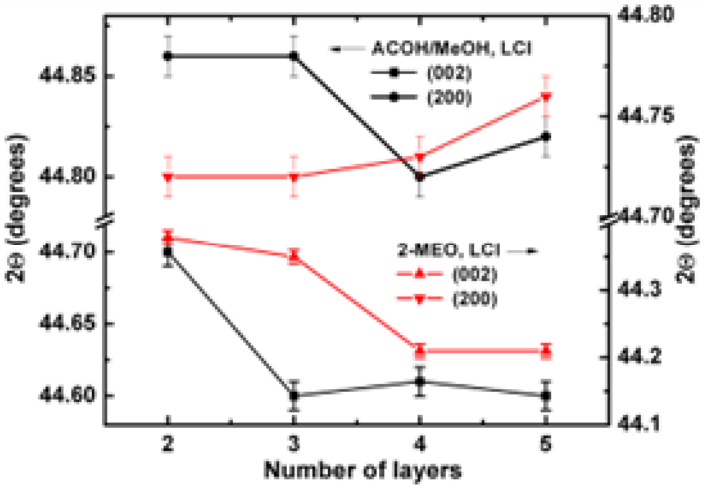
ACOH/MeOH, LCI
(002)
(200)
2-MEO, LCI
(002)
(200)
2Θ (degrees)
Number of layers

Fig. 4.

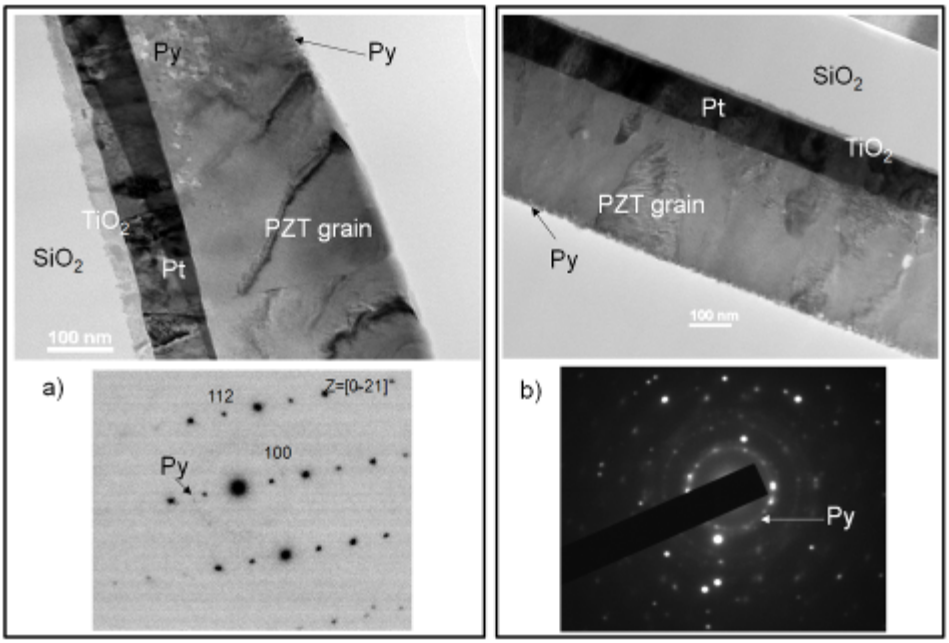
Py
Py
TiO2
SiO2
Pt
PZT grain
100 nm
a)
112
Z=[0-21]*
Py
100
SiO2
Pt
TiO2
PZT grain
Py
100 nm
b)
Py

Fig. 5.